BIOCHEMISTRY
including biophysical chemistry & molecular biology
Article

Biochemistry **2009,** *48,* 10509–10521 10509
DOI: 10.1021/bi901311p

Structure of Chemokine-Derived Antimicrobial Peptide Interleukin-8α and Interaction with Detergent Micelles and Oriented Lipid Bilayers[†,‡]

Sarah Bourbigot,[§] Liam Fardy,[§] Alan J. Waring,[⊥] Michael R. Yeaman,[⊥,@] and Valerie Booth*[,§,∥]

[§]*Department of Biochemistry and* [∥]*Department of Physics and Physical Oceanography, Memorial University of Newfoundland, St. John's, Newfoundland A1B 3X9, Canada,* [⊥]*Department of Medicine, Geffen School of Medicine, University of California, Los Angeles, California 90024, and* [@]*Division of Infectious Diseases, LAC-Harbor UCLA Medical Center, Torrance, California 90502*

Received July 29, 2009; Revised Manuscript Received October 7, 2009

ABSTRACT: Interleukin-8α (IL-8α) is an antimicrobial peptide derived from the chemokine IL-8. Solution NMR was used to determine the atomic-resolution structure of IL-8α in SDS micelles. Solid-state NMR and tryptophan fluorescence were used to probe the interaction of IL-8α with model membranes. The peptide interacted differently with anionic versus purely zwitterionic micelles or bilayers. Tryptophan fluorescence demonstrated a deeper position of Trp4 in SDS micelles and POPC/POPG bilayers compared to pure POPC bilayers, consistent with ^{2}H order parameters, which also indicated a deeper position of the peptide in POPC/POPG bilayers compared to POPC bilayers. Paramagnetic probe data showed that IL-8α was situated roughly parallel to the SDS micelle surface, with a slight tilt that positioned the N-terminus more deeply in the micelle compared to the C-terminus. ^{15}N solid-state NMR spectra indicated a similar, nearly parallel position for the peptide in POPC/POPG bilayers. ^{31}P and ^{2}H solid-state NMR demonstrated that the peptide did not induce the formation of any nonlamellar phases and did not significantly disrupt bilayer orientation in aligned model membranes composed of POPC or POPC and POPG.

Antimicrobial peptides (AMPs)[1] have been studied for several years because of their ability to kill microbes, often by targeting and disrupting their membranes (*1*). More recently, it has been recognized that AMPs can have dual functions that involve direct and indirect host defense roles. There are antimicrobial peptides that act directly against microbes but are also able to modulate the host immune response (*2*). Moreover, there are well-characterized components of the immune system, such as chemokines, for which direct antimicrobial properties have now been identified (*3*, *4*). This study concerns the structure−activity relationships of one such peptide, IL-8α, derived from the helical region of the chemokine interleukin-8 (IL-8). IL-8 is a 72-residue dimeric chemokine produced primarily by macrophages, in response to an inflammatory stimulus. NMR (*5*, *6*) and crystallography (*7*) structural studies have demonstrated that its two monomers associate to form two antiparallel α-helices sitting on a six-stranded β-sheet.

There has been much recent interest in AMPs largely because of the possibility that they could be useful as adjunctives or alternatives to traditional antibiotics. In this respect, AMPs have broad antimicrobial spectra, are active against organisms refractory to many classical antibiotics, and may exert one or more mechanisms of action that differ from traditional antibiotics (*8*). Antimicrobial peptides of human origin are of particular interest as they represent highly attractive templates for novel anti-infective therapeutics in humans. A number of AMPs present in mammals have been studied, including lactoferrin, cathelicidin, and defensins (*9*). α-Defensins (*10*) share a conserved CXC motif, which is also found in chemokines. This similarity suggested that chemokines could exert antibacterial activity, and this was indeed shown to be the case for platelet basic peptide/CXCL7 and its derivatives CTAP-3 and NAP-2 (*11*), for platelet factor-4/CXCL4 family polypeptides and RANTES/CCL5 (*12*), for MIG/CXCL9, IP-10/CXCL10, and I-TAC/CXCL11 (*3*, *13*), and for the kinocidins GRO-α/CXCL1, I-309/CCL1, MCP-2/CCL2, and lymphotactin/CL1 (*14*). Direct antimicrobial activity has also been detected for additional chemokines, including macrophage inflammatory protein-3α/CCL20 (*15*), CCL28 (*16*), granulocyte chemotactic protein 2/CXCL6 (*17*), and CXCL14 (*18*). Yang et al. identified an in vitro antimicrobial activity for 17 of the 30 human chemokines they tested (*15*). Several peptides derived from the C-terminal helical region of chemokines have also been shown to exert antimicrobial activity, such as thrombocidins TC-1 and TC-2, derived from CXCL7 (*19*), and CDAP-4, derived from CCL13 (*20*), and peptides with antimicrobial activity are also generated by the thrombin cleavage of human platelets CXCL4, CCL5, and CTAP-3 (*21*). Some antimicrobial peptides have been

[†]This work was supported by an NSERC grant to VB. Support for these investigations was also provided in-part by grants from the National Institutes of Health (AI-39001 [M.R.Y] and AI-48031 [M.R.Y and A.J.W.]). Portions of these investigations were conducted at the Los Angeles Biomedical Research Institute at Harbor-UCLA Medical Center, Torrance, CA.

[‡]The chemical shifts for IL-8α in SDS micelles can be found on the BMRB database as entry 20044.

*To whom correspondence should be addressed: Department of Biochemistry, Memorial University of Newfoundland, St. John's, Newfoundland AIB 3X9, Canada. Phone: (709) 737-4523. Fax: (709) 737-2422. E-mail: vbooth@mun.ca.

[1]Abbreviations: AMP, antimicrobial peptide; CFU, colony-forming unit; CP, cross-polarization; CSI, chemical shift index; 16-DSA, 16-doxyl-stearic acid; DOSY, diffusion-ordered spectroscopy; DSS, 0.2 mM 2,2-dimethyl-2-silapentane-5-sulfonate (sodium salt); PFG, pulsed field gradient; POPC, palmitoyl-2-oleoyl-*sn*-glycero-3-phosphocholine; POPE, phosphatidylethanolamine; POPG, 1-palmitoyl-2-oleoyl-*sn*-glycero-3-[phospho-*rac*-(1-glycerol)] (sodium salt); SUV, small unilamellar vesicle.

Published on Web 10/08/2009

developed as analogues of chemokine domains, like platelet microbicidal protein 1, which is analogous to the C-terminal regions of human platelet factor-4/CXCL4 and IL-8 (*22*−*25*).

In common with many previously characterized AMPs, several chemokines and chemokine-derived peptides present large positive patches on their surface, leading to the suggestion that they might permeabilize bacterial membranes via interactions with negatively charged bacterial membrane components (*15*). Indeed, the chemokine-derived peptide CDAP-4 has been shown to affect the surface of *Pseudomonas aeruginosa* and might thus insert itself into the bacterial membrane (*20*). However, for TC-1 and TC-2, membrane potential measurement experiments showed that these proteins do not dissipate the bacterial membrane potential. It was thus postulated that their microbial target might be intracellular (*19*). The antibacterial activity of thrombin-induced platelet microbicidal protein-1, which is an orthologue of the chemokine hPF-4, involves both the interaction with the cell membrane and the interference with intramolecular targets (*26*, *27*). Hence, further studies to elucidate the molecular mechanism(s) of chemokine-derived AMPs are necessary to improve our understanding of these important host defense molecules.

Peptide IL-8α consists of the C-terminal α-helix of IL-8 and has been shown to exert antimicrobial activity (*14*, *28*). Although there are, as yet, no published reports detailing the possibility that IL-8α or a similar peptide is produced in vivo, this does not seem unlikely given that acid hydrolysis experiments generate a peptide that consists of the IL-8α sequence with an extra proline at its N-terminal end (*28*). Moreover, there are many examples of antimicrobial peptides that are produced by cleavage of a precursor protein (*29*). Indeed, C-terminal domains of IL-8, PF-4, and other kinocidins are deployed from their respective holoproteins in vitro when subjected to proteases relevant to settings of tissue injury or infection (M. R. Yeaman et al., unpublished data) (*30*). IL-8α exerts antimicrobial activity against both Gram-negative (*Escherichia coli*, *Salmonella enterica* MR10, *Klebsiella pneumoniae*, and *Helicobacter pylori*) and Gram-positive (*Streptococcus pyogenes*) bacteria (*14*, *28*). Some of these bacteria, such as *E. coli* and *K. pneumoniae*, have been shown to be resistant to many conventional antibiotics, and thus, developing new therapeutics targeting these and other multidrug-resistant pathogens is especially important. Yount et al. have shown that IL-8α retains its antimicrobial properties in human blood and blood matrices ex vivo (*14*), an important characteristic for a therapeutic molecule. Solid-phase assays, performed by measuring the diameter of inhibition zones, have been used to determine a lethal concentration of ∼60 μM for IL-8α, which is comparable with the lethal concentration of ∼55 μM of the cecropin-like peptide Hp(2−20). Activity in the presence of salt is another important characteristic in a therapeutic molecule. Like many antibacterial peptides such as indolicidins (*31*), gramicidins, and magainins (*32*), IL-8α had a reduced activity at higher NaCl concentrations and completely lost its antimicrobial activity at 350 mM NaCl. However, at 255 mM NaCl, IL-8α appeared to be relatively salt-resistant as it still retained ∼60% of its activity (*28*), compared to the 65% of the activity of CXCL14 at 100 mM NaCl (*18*), and GCP-2/CXCL6, which showed complete abrogation of antimicrobial activity at 100 mM NaCl (*17*). When the pH was decreased from 7.4 to 5.0, IL-8α exerted a stronger antibacterial activity. In inhibition zone assays performed by Björstad (*28*) and Cole (*3*) or in colony-forming assays (*15*), no measurable antimicrobial activity could be observed for full-length IL-8 against *E. coli*, *Listeria monocytogenes*, or *Staphylococcus aureus* at pH 7.4−7.5. On the other hand, in solid-phase assays performed at pH 5.5, Yount et al. (*14*) showed full-length IL-8 exerts not only an antibacterial activity against *Salmonella typhimurium* and modest activity against *S. aureus* but also antifungal efficacy equivalent to that of defensin hNP-1 against *Candida albicans*. Importantly, in solution-phase studies at pH 5.5 and 7.5, the IL-8α peptide exerted strong candidacidal activity, whereas its antibacterial efficacy was comparably lower (*24*). These activity profiles were conferred by the IL-8α peptide, in a manner autonomous from the N-terminal regions of the IL-8 holoprotein.

We have previously studied the structure of RP-1, a synthetic antimicrobial peptide designed on the basis of the C-terminal α-helix of the chemokine platelet factor-4/CXCL4 (*33*). Similar structures were obtained for RP-1 in complex with micelles composed of SDS, which roughly mimic anionic bacterial membranes, and DPC, which approximate zwitterionic eukaryotic membranes. This observation led to the suggestion that RP-1's preferential specificity for bacterial versus mammalian membranes is likely due to differences in the mode of the lipid−peptide interaction rather than differences in peptide structure in the two environments. Thus, for the IL-8α peptide, we chose to limit the solution NMR structural studies to a single micelle system, SDS, and focus on its interactions with bilayers using solid-state NMR of oriented lipid bilayers. Additionally, tryptophan fluorescence studies were performed to elucidate the role of the tryptophan residue in the bilayer interactions, as well as to allow the direct comparison of IL-8α's interactions with micelles and bilayers, as this technique can be used on both contexts.

MATERIALS AND METHODS

Materials. The IL-8α peptide (NH_2-K^1ENWV^5QRVVE^{10}-KFLKR^{15}AENS-COOH) was produced by solid-phase synthesis using Fmoc (*O*-fluorenylmethyloxycarbonyl) chemistry. ^{15}N labels were incorporated at positions V5, V8, L13, and A16. The peptide was purified using reversed-phase HPLC, and its mass was authenticated by MALDI-TOF spectrometry. The purity of the resulting sample was determined to be ≥95% by analytical HPLC.

Sodium dodecyl sulfate-d_{25} was obtained from Cambridge Isotope Laboratories (Andover, MA). Sodium dodecyl sulfate, 16-doxyl-stearic acid (16-DSA), and sodium azide were from Sigma-Aldrich. 1-Palmitoyl-2-oleoyl-*sn*-glycero-3-phosphocholine (POPC), 1-palmitoyl(D31)-2-oleoyl-*sn*-glycero-3-phosphocholine (POPC-d_{31}), 1-palmitoyl-2-oleoyl-*sn*-glycero-3-[phospho-*rac*-(1-glycerol)] (sodium salt) (POPG), and 1-palmitoyl(D31)-2-oleoyl-*sn*-glycero-3-[phospho-*rac*-(1-glycerol)] (sodium salt) (POPG-d_{31}) were purchased from Avanti Polar Lipids, Inc.

Circular Dichroism. The sample of IL-8α in pure water was used to run circular dichroism experiments. These were performed on a Jasco J-810 spectropolarimeter. The mean of four spectra acquired at 308 K over a range of 180−300 nm was analyzed.

Solution NMR. (*i*) *NMR Structure Determination*. Spectra were acquired on a Bruker Avance 500 MHz spectrometer equipped with *z*-gradients and a triple-resonance TXI probe, processed with NMRPipe (*34*), and analyzed using SPARKY (*35*). Two IL-8α samples were prepared in pure water and in SDS micelles. For both samples, 1.5 mM peptide was

dissolved in 90% H_2O and 10% D_2O at pH 5.0. Additionally, 0.2 mM 2,2-dimethyl-2-silapentane-5-sulfonate (sodium salt) (DSS) and 0.2 mM sodium azide were added; 150 mM deuterated SDS was added to one of the samples for the experiments in micelles. For structure analysis in water, two-dimensional (2D) $^{15}N-^{1}H$ HSQC spectra, 2D TOCSY spectra, and 2D NOESY spectra were recorded at 35 °C. For the study in micelles, samples were analyzed by 2D $^{15}N-^{1}H$ HSQC, 2D TOCSY, and 2D NOESY with mixing times varying from 100 to 200 ms and at temperatures of 25 and 35 °C. The chemical shifts were referenced with respect to DSS (0.0 ppm). Resonance frequency assignments were determined using the 2D TOCSY and NOESY spectra recorded at 35 °C (*36*). All peptide resonances that we expected to observe except K1 Hε* and Hγ*, K11 Hε*, and F12 Hζ were assigned. The N-terminal group was not observed, and it was not possible to make stereospecific assignments.

NOEs were quantified using the peak height from the 2D NOESY spectrum with a mixing time of 150 ms, at 35 °C. The NOEs were divided into three classes corresponding to strong, medium, and weak intensities and assigned target distances of 1.8−2.5, 1.8−3.5, and 1.8−5 Å, respectively (*37*). For structure calculations, hydrogen bond ($H_{i+4}\cdots O_i$ = 2.5 Å, and $N_{i+4}\cdots O_i$ = 3.5 Å) and dihedral angle ($\varphi = -60 \pm 30°$, and $\phi = -40 \pm 40°$) restraints were defined for the segment where NOE patterns clearly indicated an α-helix (residues 3−16). Ambiguous NOEs were used when two to six possible inter-residue assignments existed for a cross-peak. Fifty structures were calculated using the simulated annealing algorithm within CNS 1.1 (*38*). Analysis of the final structures was performed using Procheck-NMR (*39*, *40*). Structures were visualized in MOLMOL (*41*) and Swiss-Pdb Viewer (*42*).

(*ii*) *Paramagnetic Probe Experiments*. Spectra were acquired on a Bruker Avance 600 MHz spectrometer. For paramagnetic line broadening experiments, IL-8α was made up at a concentration of 1.5 mM in 90% H_2O, 10% D_2O, 150 mM SDS-d_{25} (pH 5.0), 0.2 mM DSS, and 0.2 mM sodium azide. A 0.4 M stock solution of 16-DSA in deuterated methanol was prepared. It was then mixed with the protein/micelle sample to final concentrations of 0.6, 1.2, and 2.4 mM. The maximal amount of deuterated methanol in the sample was 5 μL for a total sample volume of 600 μL. $^{15}N-^{1}H$ HSQC and TOCSY spectra were recorded at 35 °C, before and after the addition of 16-DSA. The pH of the sample was adjusted after each addition of 16-DSA.

(*iii*) *DOSY Experiments*. To determine the hydrodynamic radius (R_H) of IL-8α and SDS alone and in complex, diffusion experiments were performed. Three samples were prepared: (1) 1.5 mM IL-8α in H_2O and D_2O, (2) 1.5 mM IL-8α and 150 mM SDS-d_{25} in H_2O and D_2O, and (3) 150 mM SDS in H_2O and D_2O. For all three samples, 0.4 mM DSS and 0.4 mM NaN_3 were added and the pH was adjusted to 5.0. DOSY (diffusion-ordered spectroscopy) experiments were acquired with pulsed field gradient (PFG) NMR (*43*) on a Bruker Avance 600 MHz spectrometer, using a stimulated echo with bipolar gradient pulses (*44*), followed by a 3-9-19 pulse for water suppression (*45*). The spectra were collected in 32 steps, attenuating the signal to ~5% of the initial value by increasing the gradient strength from 2 to 95% of the maximum amplitude, for a constant diffusion time of 100 ms and an optimized gradient pulse length of 1 ms.

The spectra were processed with Bruker Topspin 2.0. Diffusion constants were derived from the following equation:

$$I = I_0 e^{-D\gamma^2 g^2 \delta^2 (\Delta - \delta/3)}$$

where I is the observed intensity, I_0 the unattenuated signal intensity, D the diffusion coefficient, γ the gyromagnetic ratio of ^{1}H, g the gradient strength, δ the gradient length, and Δ the diffusion time.

Solid-State NMR. (*i*) *Sample Preparation*. The lipids and peptide were dissolved in a $CH_3OH/CDCl_3$ mixture (1/1 in volume); 4−10 mg of POPC/POPC-d_{31}, POPC-d_{31}/POPC/POPG, or POPC/POPG/POPG-d_{31} micelles was used, with a 3/1 POPC/POPG molar ratio, and 30% of the sample (by weight) was deuterated. The solution (a total volume of 200 μL) was spread homogeneously on 12 mica plates. They were then dried for approximately 2 h in a fume hood before being placed in a vacuum chamber overnight. Each plate was then spread with 5 μL of doubly distilled water and placed in a hydration chamber with a saturated ammonia phosphate solution at 4 °C for 2 days. The plates were then stacked together, wrapped with plastic film, and sealed with polystyrene plastic. Samples were stored at 4 °C before the NMR experiments.

(*ii*) *NMR*. The spectra were acquired on a Bruker Avance solid-state NMR spectrometer operated at frequencies of 243.02, 92.15, and 60.83 MHz for ^{31}P, ^{2}H, and ^{15}N nuclei, respectively. The oriented samples were positioned with the normal to the bilayer parallel to the magnetic field. For ^{31}P and ^{15}N experiments, the sample was inserted into a Bruker dual tuned 4 mm flat coil probe, and for the ^{2}H experiments, a Bruker triply tuned 3 mm flat-coil probe was used. For ^{31}P experiments, a proton-decoupled experiment was conducted with a 90° pulse length of 12 μs. Other acquisition parameters were as follows: recycle delay of 5 s, SPINAL-64 proton decoupling strength of 65 kHz, spectral width of 200 ppm, and a total of 2888 scans. The chemical shift was externally referenced to 85% H_3PO_4 as 0 ppm. For ^{15}N experiments, a cross-polarization (CP) pulse sequence was used, with TPPM proton decoupling (*46*). Using 1024 data points, 65498 scans were acquired with a CP contact time of 6 ms and a recycle delay of 5 s. For ^{2}H experiments, a quadrupole echo pulse sequence ($\pi/2-\tau-\pi/2-\tau-$acq) was used with $\pi/2$ and τ set to 2.5 and 15 μs, respectively; 10240 scans were acquired, and the recycle delay was 1 s. The spectral width was 200 kHz. The experiments were performed at 20 °C.

(*iii*) *Order Parameter Calculation*. The deuterium spectra enabled us to calculate the order parameters for the carbon acyl chains. The peaks in these spectra were assigned with the appropriate carbon positions of the (*sn*-1) acyl chain. The center pair is attributed to the deuterons on the methyl group, which have the more flexible motion. Then, the following pair is contributed by deuterons next to the methyl group (C15) and so on for deuterons on C14, C13, C12, and C11, which have larger splittings because they are closer to the headgroup and consequently have more constrained motion. The order parameter changes slowly along the chain, which is characterized by an overlap of the doublets on the ^{2}H NMR spectrum. The dependence of orientational order on position can be estimated by the smoothed order parameter profile approach (*47*). In this unresolved region of the spectrum, called the orientational order parameter plateau, the peak positions are approximated by dividing the spectrum corresponding area into nine equal parts and assuming that the quadrupole splitting changes

monotonically with position along the chain. The order parameters can then be calculated using the following formula

$$\Delta\nu_{CD^i} = \frac{3\nu_{CD}}{2} S_{CD^i}$$

where $\Delta\nu_{CD^i}$ is the quadrupole splitting of deuterons at the ith carbon position of the acyl chain, ν_{CD} the quadrupole coupling constant of deuterium [167 kHz in deuterated paraffin hydrocarbons (*48*)], and S_{CD^i} the order parameter.

Fluorescence Experiments. We prepared small unilamellar vesicles (SUVs) by mixing the lipids in chloroform (10 mg/mL) and drying off the solvent under a stream of nitrogen gas and then under vacuum overnight. The samples were then resuspended in H_2O to create a 0.1 M lipid stock solution. The lipid suspension was frozen and thawed five times before being sonicated in a water bath sonicator until the solution became opalescent.

Steady-state fluorescence spectra were recorded using a Shimadzu RF-540 spectrofluorometer. Measurements were performed with an excitation wavelength of 295 nm to avoid the fluorescence of other aromatic residues and to reduce the absorbance by acrylamide. The emission wavelength was scanned from 300 to 450 nm with 0.5 nm increments, in a 3 mm × 10 mm quartz cell at room temperature. Both the excitation and emission slit widths were set to 5 nm. Spectrum baselines were corrected by subtracting the blank spectra of the detergent or lipid solution without peptide. The concentration of peptide was 2 μM, and experiments were performed in the presence or absence of 25 mM SDS or 5 mM lipid vesicles. Quenching experiments were conducted via addition of increasing concentrations of acrylamide (from 10 to 200 mM). The emission was monitored at the peak obtained from the spectra in the absence of quencher. The effect of acrylamide on the peptide was analyzed using the Stern−Volmer equation (*49*)

$$F_0/F = 1 + K_{SV}Q$$

where F_0 and F are the fluorescence intensity in the absence and presence of the quencher, respectively, K_{SV} is the Stern−Volmer quenching constant, and Q is the quencher concentration.

RESULTS

Structure of IL-8α in Aqueous Solution. Circular dichroism experiments were conducted for IL-8α in aqueous solution. Overall, the CD spectra were characteristic of random coil conformation (data not shown), but an inflection point near 222 nm suggested a propensity to structure as α-helix (*50*). This α-helical propensity was further substantiated by the NMR experiments. The one-dimensional (1D) proton and 2D $^{15}N-^{1}H$ HSQC spectra (not shown) exhibited more dispersion of the peptide amide proton chemical shifts than expected for a peptide in a random coil conformation. In the NOESY spectrum, we observed strong HN−HN correlations, which are indicative of α-helical structure.

Structure of IL-8α in SDS Micelles. The three-dimensional (3D) structure of IL-8α was determined in SDS micelles using solution NMR. 1D proton and $^{15}N-^{1}H$ HSQC spectra were acquired at 25, 30, and 35 °C; 35 °C was chosen for the structural analysis as the peptide exhibited the least conformational inhomogeneity at that temperature. 2D TOCSY and 2D NOESY experiments were thus conducted at 35 °C. The strong HN_i-HN_{i+1} NOEs and the HN_i-HN_{i+2} NOEs, added to the various $H\alpha_i-HN_{i+3}$ and $H\alpha_i-H\beta_{i+3}$ correlations, indicated an

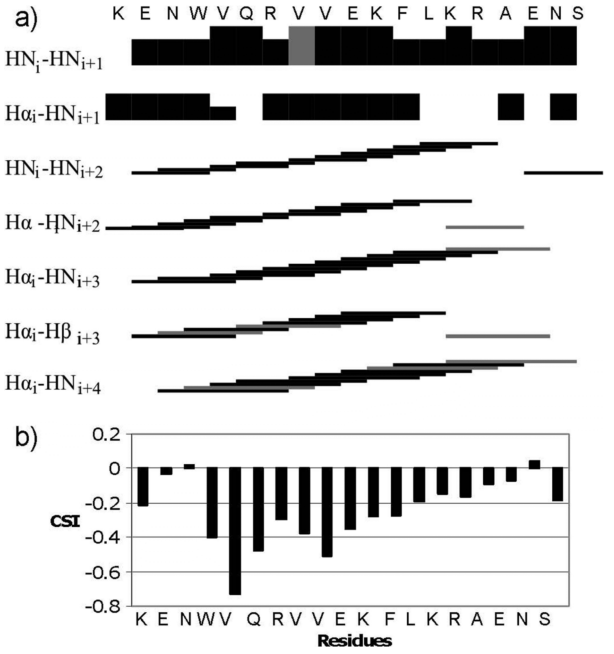

FIGURE 1: Secondary structure indicators for IL-8α. (a) Black bars indicate unambiguously assigned NOEs, and gray bars represent ambiguous NOEs. For sequential NOEs, the height of the bars corresponds to the intensity of the NOE. (b) Chemical shift indices (CSIs) for IL-8α (*51*).

α-helical conformation for residues 3−16. This was supported by the chemical shift index (CSI) values, the difference between the Hα proton chemical shifts in the SDS environment and the chemical shifts in a random coil (*51*) (Figure 1). The CSI values indicate a helical structure for residues 3−17 with a weakening of the helix toward the C-terminal end.

Structure calculations were performed using the NOE-derived distances. α-Helical hydrogen bond and dihedral angle restraints were also added for residues 3−16. An ensemble of 50 structures was calculated using 86 sequential, 113 medium-range, and 42 ambiguous NOEs. Of this ensemble, the 10 lowest-energy structures were retained for analysis. An average of ~12 restraints per residue allowed for good definition of the structure, with a backbone rmsd (root-mean-square deviation) of 0.89 Å. Ninety-two percent of the residues fell within the most favored region of the Ramachandran plot, while no residues were found in the disallowed region (Table 1). The calculated structure displays a well-defined α-helix for residues 3−16 (Figure 2). The N- and C-terminal residues are more flexible because of their position at the end of the peptide. The side chains orient in a way that makes the helix amphipathic.

Peptide−Micelle Interactions. To further probe the IL-8α−SDS micelle interaction, diffusion NMR experiments were performed to determine the translational diffusion coefficient of the SDS micelles and IL-8α peptide alone and in complex (see the Supporting Information). When the peptide was alone in solution, the values were 0.98×10^{-10} and 3.23×10^{-10} m^2/s for SDS micelles and IL-8α, respectively. The results for SDS alone in solution are consistent with the known size of SDS micelles (*52*, *53*). The diffusion constant for the complex was found to be 2.46×10^{-10} m^2/s as measured using the IL-8α peaks. The reason the complex appears to diffuse faster than an SDS micelle alone may be a result of fast exchange of the peptide between bound and unbound states, making the peptide's observed diffusion

constant a weighted average of the bound and unbound diffusion constants (*54*, *55*).

To assess the position of IL-8α within the SDS micelles, 16-DSA was added to the peptide/micelle sample. This paramagnetic probe incorporates into the micelles with its free radical group positioned close to the center of the micelle, inducing a broadening and thus a height reduction of signals for the protons that are close to the micelle center (*56*, *57*). A line width broadening was observed for the entire spectrum of the peptide after 16-DSA was added, as expected for a peptide bound close to the surface of micelles. The intensity reduction of Hα−HN and Hβ−HN correlations was monitored in TOCSY spectra and compared to the average intensity reduction (Figure 3). The data for Hα−HN correlations from K1, Q6, V8, and E17 and for Hβ−HN correlations from K1, Q6, R7, V8, E10, K14, E17, and S19 were not retained in the analysis because they exhibited signal overlap. The protons experiencing a reduction in signal intensity close to the average were not plotted on the structure. The remaining residues were grouped as either exhibiting a larger or a smaller reduction in intensity than the average value. The former are thus located facing inside the micelles, while the latter face the exterior of the micelle. This information was mapped on the structure displayed in Figure 2b. Most of the residues closest to the DSA probe localize to one face of the helix, consistent with IL-8α being positioned roughly parallel to the micelle−water interface. However, the N-terminal residues were more affected by the 16-DSA than the C-terminal residues. Thus, it seems that the peptide inserts itself into the SDS micelle with a slight angle, leaving the C-terminus and the exterior face of the C-terminal end of the helix outside the micelle.

Tryptophan Fluorescence Quenching in Micelles and Vesicles. The aromatic ring of the tryptophan at position 4 is located on the hydrophobic face of IL-8α, but near the juncture between the hydrophobic and hydrophilic faces (Figure 2b), and is thus likely to be positioned at the interfacial region between the

Table 1: NMR Structure Calculation Parameters[a]

no. of restraints used in structure calculation	
total NOE	242
sequential ($i - j = 1$)	86
medium-range ($\|i - j\| \leq 4$)	114
ambiguous	42
hydrogen bond	24
dihedral angle	31
CNS energy (kcal/mol) for the ensemble of 10 lowest-energy structures	
$E_{overall}$	58.27 ± 7.9
E_{bond}	2.75 ± 0.5
E_{angle}	25.92 ± 3.37
$E_{improper}$	4.22 ± 1.42
E_{vdw}	14.24 ± 1.86
E_{noe}	11.06 ± 1.51
E_{cdih}	0.07 ± 0.15
no violations of >0.4 Å	
Ramachandran plot summary (%)	
most favored	91.8
additionally allowed	3.5
generously allowed	4.7
disallowed	0
average rmsd from mean structure (Å)	
backbone atoms	0.899
all heavy atoms	1.416

[a]The default parameters and force constants of protein-allhdg.param and anneal.inp in CNS 1.1 were used for calculation.

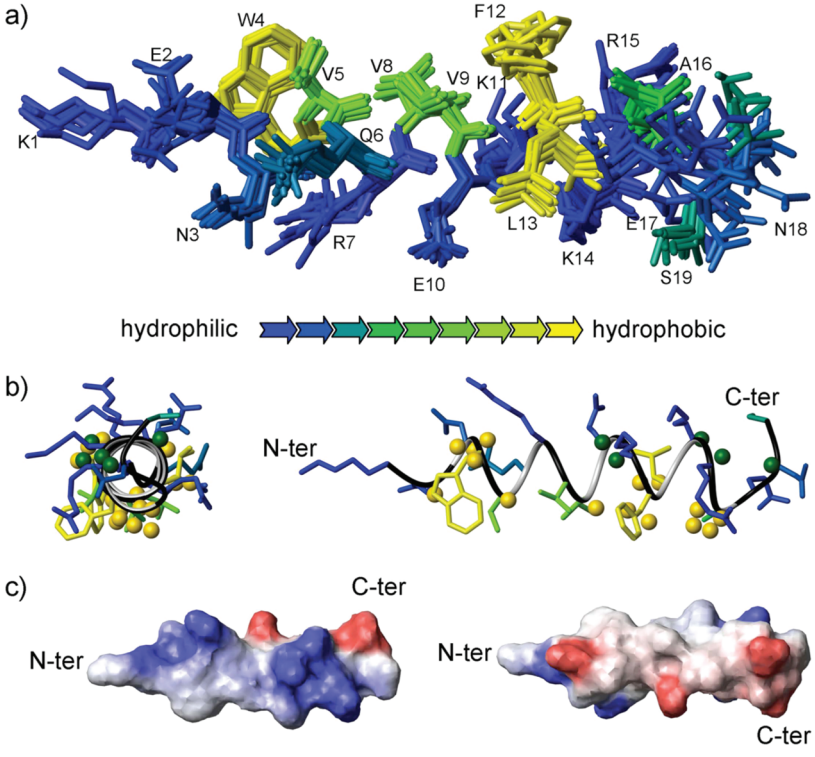

FIGURE 2: Structure of IL-8α. (a) Ensemble of the 10 lowest-energy structures of IL-8α. The structures were superimposed using the backbone atoms of residues 3−16. The amino acids are colored according to hydrophobicity (see the key for the color scheme). (b) Ribbon representation of the structure of IL-8α with the lowest energy (side view on the left). Spheres represent the results of the paramagnetic probe experiments: Hα and Hβ atoms located closer to the micelle interior are represented as yellow spheres, whereas Hα and Hβ atoms located closer to the micelle exterior are represented as green spheres. (c) Electrostatic potential surface representation of the two opposite faces of the IL-8α representative structure with blue and red for positive and negative charge, respectively, and white for nonpolar.

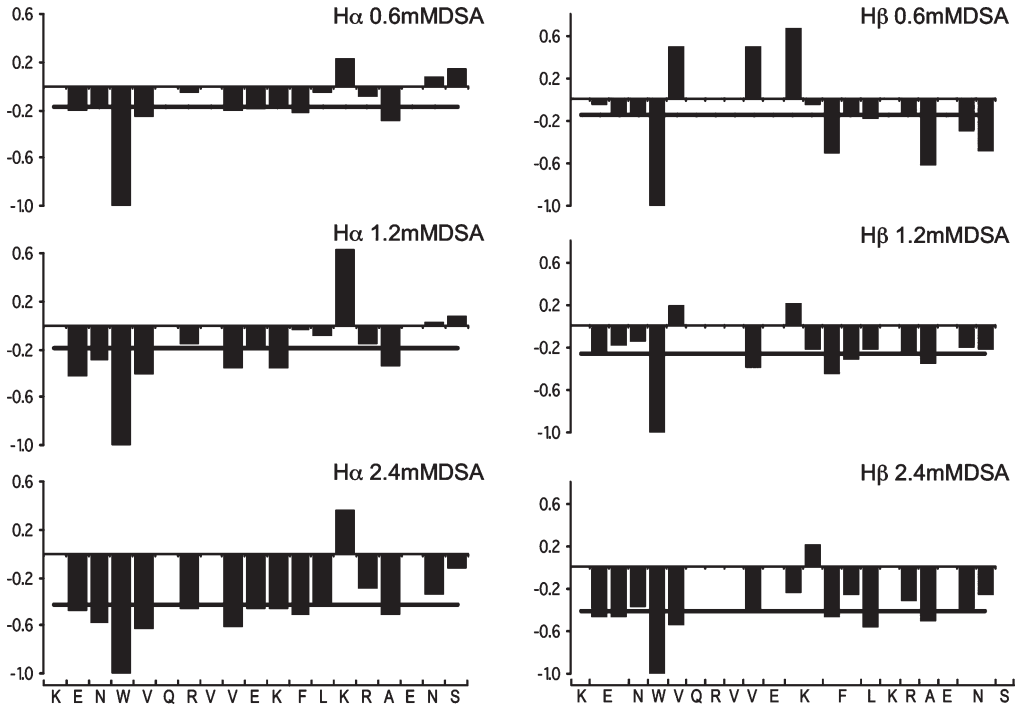

FIGURE 3: Effect of 16-DSA on IL-8α. The ratio of 2D TOCSY cross-peak intensity with and without 16-DSA is plotted along the amino acid sequence at 0.6 (top), 1.2 (middle), and 2.4 mM 16-DSA (bottom), together with the average values at each 16-DSA concentration, represented as a black line, for Hα protons on the left and Hβ protons on the right.

micelle and the water. Tryptophan fluorescence experiments were conducted to characterize the interaction of this residue with micelles, as well as bilayers.

Emission spectra of IL-8α were recorded in the presence and absence of detergents or lipids. In pure H_2O, the maximum fluorescence emission was observed at 350 nm. When POPC SUVs were added, only a small intensity increase was observed and the maximum emission remained close to 350 nm (data not shown). This indicates the tryptophan remains in a polar environment when the peptide is bound to POPC SUVs (*58*). When SDS micelles or POPC/POPG SUVs were added, the fluorescence intensity increased markedly and we observed a blue shift of the tryptophan fluorescence (maximum peak at 336 nm in SDS and 332 nm in POPC and POPG) (*59*). This indicates a more hydrophobic environment surrounding the tryptophan in SDS micelles and POPC/POPG SUVs as compared to pure POPC SUVs, consistent with a deeper insertion of the tryptophan into the anionic micelles and SUVs.

To gain further insight into the peptide insertion, we added increasing concentrations of acrylamide to the samples and measured the reduction in tryptophan fluorescence intensity. Acrylamide is a polar and uncharged compound, and thus, it remains in solution and does not extensively affect the fluorescence of tryptophan if it is buried in the lipid phase. Figure 4 shows the Stern−Volmer plots of fluorescence quenching and the Stern−Volmer constants calculated from these plots. The tryptophan was readily quenched in pure water, indicating that it is easily accessible in the solution. When the peptide was in complex with SDS detergent micelles or lipid SUVs, the tryptophan fluorescence was less affected by the addition of acrylamide. K_{SV} values, which indicate the extent of Trp's exposure to solution, were calculated for IL-8α in the various environments. The K_{SV} values calculated for IL-8α in the presence of SDS micelles and POPC/POPG SUVs are significantly lower than the K_{SV} in the presence of POPC SUVs. Under the former conditions, the tryptophan is more protected from the acrylamide quenching than under the latter conditions. These results show that the tryptophan inserts deeply into anionic micelles or lipid SUVs, whereas in the POPC SUVs, it remains either more accessible to the solvent or in a very hydrophilic environment. The K_{SV} values are almost the same in SDS micelles and in POPC/POPG SUVs, indicating that the tryptophan is equally protected in both environments.

Solid-State NMR of IL-8α in Oriented Lipid Bilayers. Interactions with membranes are critical aspects of AMP function, whether they act by disrupting membranes or merely pass through membranes on their way to an intracellular target. Hence, we used solid-state NMR to assess the impact of IL-8α on lipid bilayers composed of POPC, to mimic mammalian membranes, or POPC and POPG, to mimic bacterial membranes. We examined the effects of the peptide on lipid bilayers by acquiring ^{31}P and ^{2}H NMR spectra of oriented lipids without peptide and with 3 and 6% (by mole) peptide.

First, to study the interaction of IL-8α with the lipid headgroups, as well as the effect of the peptide on overall bilayer orientation, we performed ^{31}P experiments. For lipids alone, the major peaks were observed at 36.4 and 39 ppm for the POPC and POPC/POPG samples, respectively, with a minimal signal from 0 to −12 ppm (Figure 5), indicating that in the absence of peptide, the lipid bilayers were well-aligned. Addition of 3 or 6 mol % peptide to the POPC bilayer did not appear to increase the ratio of unaligned species, indicating that the peptide did not perturb the bilayer alignment. There was a small decrease in the chemical shift of the major ^{31}P peak with addition of peptide. ^{31}P MAS experiments indicated no peptide-induced change in isotropic chemical shift or line width, which would suggest a change in headgroup dynamics (Figure 2 of the Supporting Information). The MAS data imply that the source of the small shift seen in the oriented, static spectra is likely a change in headgroup tilt, which is consistent with a peripheral association of the peptide with the

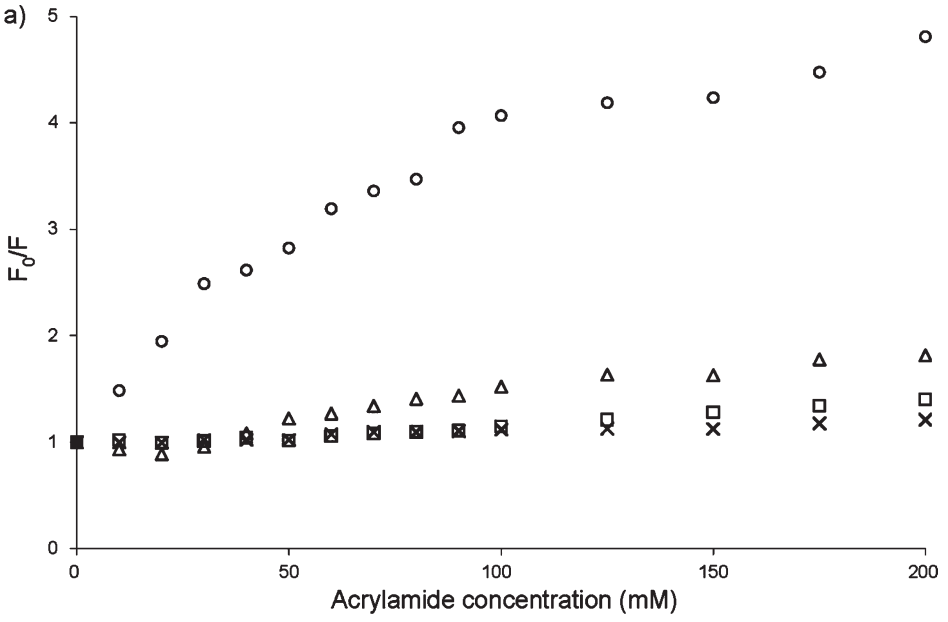

b)

	H_2O	SDS	POPC	POPC/POPG
K_{SV} in M^{-1} (R^2 value is given in brackets)	24.1 (0.68)	1.7 (0.9)	4.4 (0.91)	1.0 (0.93)

FIGURE 4: Tryptophan fluorescence quenching by acrylamide. Stern−Volmer plots (a) and constants (b) of IL-8α for acrylamide quenching experiments in pure H_2O (○) and bound to SDS micelles (□), POPC SUVs (△), and POPC/POPG SUVs (×).

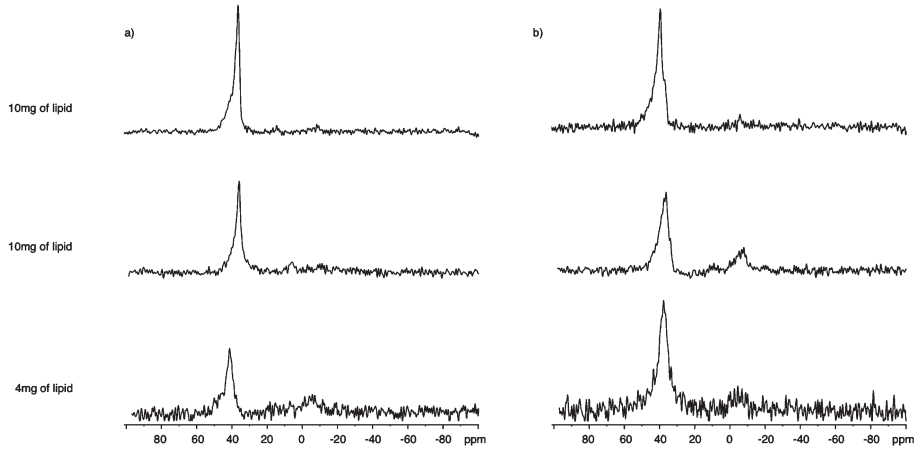

FIGURE 5: ^{31}P spectra of mechanically oriented bilayers of (a) POPC and POPC-d_{31} (7/3, w/w) and (b) POPC-d_{31} and POPG (3/1 molar ratio) in the absence (top) and presence of 3 (middle) and 6 mol % IL-8α (bottom). The vertical scale of each spectrum was corrected according to the relative amount of lipids that were used to prepare the sample. The bilayers were oriented with the bilayer normal along the magnetic field. Spectra of POPC/POPG-d_{31} bilayers were also acquired but are not shown since they appear very similar to those of POPC-d_{31}/POPG bilayers.

bilayers such that headgroup tilt is affected without modification of bilayer alignment. When peptide was added to the POPC/POPG bilayers, some increase for unaligned lipid species was seen in most samples; however, the peptide-induced perturbation of the bilayer alignment was minimal, even at relatively high peptide concentrations.

Deuterium NMR was employed to study the effects of the IL-8α peptide on the lipid chains. The ^2H spectra of POPC-d_{31}, POPC-d_{31}/POPG, and POPC/POPG-d_{31} bilayers are shown in Figure 6 in the presence and absence of IL-8α. In the absence of peptide, a symmetric spectrum with well-resolved peaks characteristic of well-aligned bilayers was obtained. When IL-8α was included in the sample, the amount of rapidly reorienting material remained very small, as indicated by the absence of strong signals at the center of the spectrum. The peaks broaden slightly as the concentration of IL-8α increases. In POPC, the inclusion of 3 mol % peptide induces a reduction in the quadrupole splitting, indicating a less restricted motion of lipid acyl chains in the presence of IL-8α. When 6 mol % peptide was added, the spectral resolution decreases dramatically (data not shown), precluding order parameter calculation. In POPC/POPG samples, IL-8α significantly reduces the quadrupolar coupling only at the highest concentration (6 mol %).

To ascertain the effect of the peptide along the lipid chain, order parameter profiles were calculated from the quadrupolar splittings in the ^2H spectra (Figure 7). In POPC, the addition of IL-8α resulted in a decrease in the order parameters for the entire lipid chain length. For the POPC/POPG mix, the degree of order

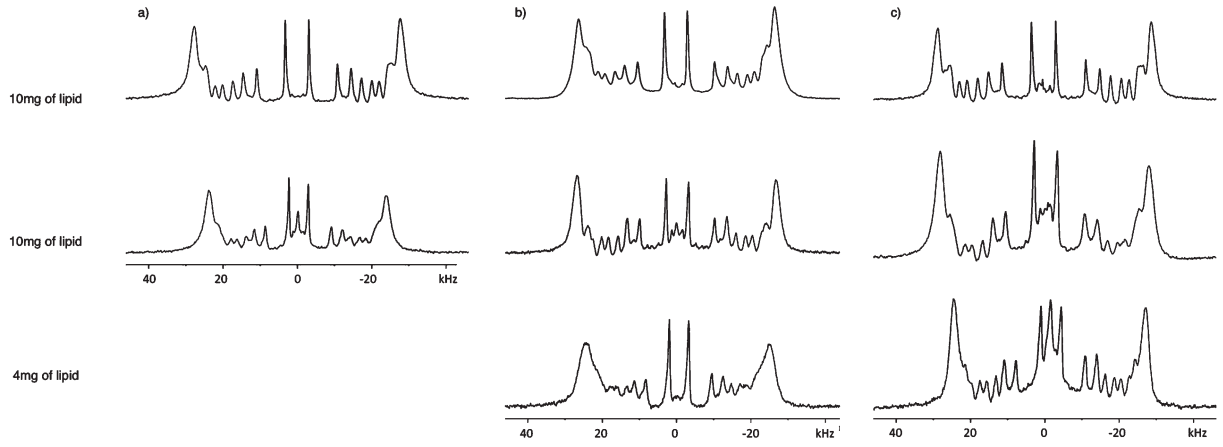

FIGURE 6: ^{2}H spectra of mechanically oriented bilayers composed of (a) POPC and POPC-d_{31} (7/3, w/w), (b) POPC-d_{31} and POPG (3/1 molar ratio), and (c) POPC and POPG-d_{31} (3/1 molarratio) in the absence (top) and presence of 3 (middle) and 6% IL-8α (bottom). The vertical scale of each spectrum has been corrected according to the relative amount of lipids that were used to prepare the sample. The bilayers were oriented with the bilayer normal along the magnetic field.

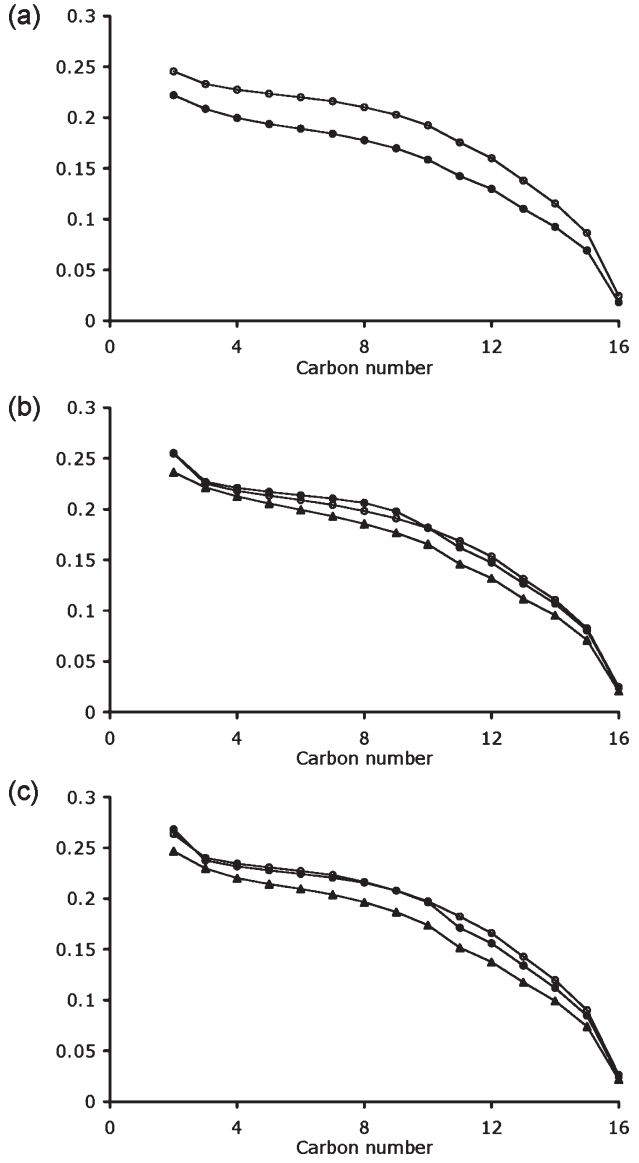

FIGURE 7: Order parameter profiles of the *sn*-1 chains of POPC-d_{31} in POPC/POPC-d_{31} samples (a), of POPC-d_{31} in POPC-d_{31}/POPG samples (b), and of POPG-d_{31} in POPC/POPG-d_{31} samples (c), in the absence (○) and presence of 3 (●) and 6% IL-8α (▲). Data derived from Figure 6.

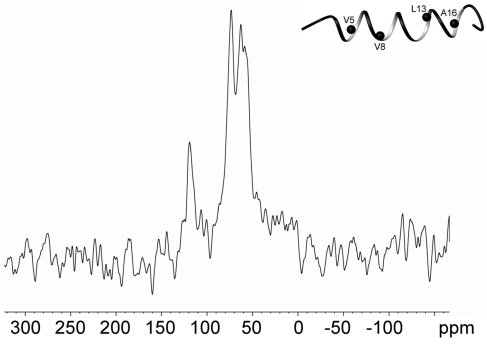

FIGURE 8: ^{15}N spectrum of mechanically oriented 3/1 POPC-d_{31}/POPG bilayers, with 3 mol % IL-8α. The inset shows a ribbon representation of the representative structure of SDS-bound IL-8α with ^{15}N atoms as black spheres.

did not change when 3% IL-8α was added, using either POPC or POPG as the deuterium-labeled species. In POPC/POPG samples, a slight decrease in the order parameters could be observed once 6% IL-8α was included.

As there are four residues enriched with ^{15}N in the peptide (V5, V8, L13, and A16), it was possible to run static ^{15}N cross-polarization spectra of IL-8α in oriented bilayers (Figure 8). This experiment gives the anisotropic chemical shits for these atoms, which depend on the orientation of the helical axis with respect to the bilayer normal. Chemical shifts of < 100 ppm correspond to an in-plane alignment, while chemical shifts in the 200 ppm region indicate a transmembrane orientation (*60*). In the ^{15}N spectrum of the sample with 10 mg of POPC-d_{31}/POPG bilayers and 3% IL-8α, there are three peaks in the ~60−70 ppm range and a fourth close to 120 ppm. It may be that the 120 ppm peak corresponds to A16 since this is the terminal residue of the helix and thus may deviate more from the canonical angles than the other three residues that are in the more regular part of the helix. In any case, that most of the ^{15}N signal is less than 100 ppm indicates a predominantly in-plane alignment for the helix.

DISCUSSION

Compared to most antimicrobial peptides found in the Antimicrobial Peptide Database, IL-8α has a rather modest positive charge (+2 as compared to the average of +4.4) and hydrophobic content (36% as compared to the average of 48%) (*61*). These

distinctive physicochemical attributes provide a special context in which to contemplate the molecular mechanisms of this peptide, which has been shown to exert an antibacterial activity against both Gram-negative and Gram-positive bacteria (*14*, *28*). We started by assessing the structure of IL-8α in water and in complex with SDS micelles that approximate prokaryotic membranes. In pure water, circular dichroism and NMR spectra indicated that IL-8α is largely random coil in conformation, but with an apparent propensity for α-helical conformation. Upon interaction with SDS micelles, IL-8α assumes a well-defined, highly amphipathic α-helix spanning residues 3−16 (Figure 2). These results are in line with previous studies of antimicrobial peptides that exhibit disorder in aqueous solution but structure upon binding to detergent micelles (*33*, *62*, *63*). Comparison of the structure of IL-8α in SDS micelles with the structure of this fragment within the context of the entire IL-8 protein (*5*−*7*) demonstrates that this region is structured similarly in both cases, with only small differences in side chain orientation.

It was also of interest to investigate the spatial orientation through which IL-8α interacts with target lipid systems. The paramagnetic probe data indicate that IL-8α is oriented with its helical axis roughly parallel to the SDS micelle−water interface, but with a slight angle that positions the N-terminal residues more deeply in the micelles than the C-terminal residues (Figure 2b). This finding is consistent with the extended structure adopted by Lys1 and Arg7, which may allow the positively charged termini of their side chains to be positioned close to the micelle surface, while their backbone and aliphatic chain atoms remain buried within the micelle. This so-called "snorkeling" phenomenon has been observed previously (*64*, *65*) and is hypothesized to be important for the interaction between protein and lipids (*66*). On the basis of the position of IL-8α within the micelle, combined with the dispensation of the side chains in the structure (Figure 2b), it seems reasonable to speculate that the tryptophan at position 4 may be the entity responsible for drawing the N-terminus of the peptide further toward the micelle interior.

Tryptophan itself is an amphipathic residue (*67*), having a side chain with both polar and hydrophobic groups and thus a tendency to be positioned at interfaces (*68*). Tryptophan residues have been shown to be critical for the activity of several antimicrobial peptides (*69*, *70*), related to their role in anchoring peptides in membranes and stabilizing peptide structure in bilayers (*71*, *72*). Some antimicrobial peptides are rich in tryptophan, a composition that enables them to disrupt bacterial membranes (*73*, *74*). In bovine lactoferricin, the substitution of Trp6 or Trp8 with alanine leads to a dramatic decrease in antibacterial activity (*75*). However, even if tryptophan facilitates membrane insertion, it is likely that other processes (e.g., electrophoretic) contribute to transmigration of such peptides across the membrane if they are to reach intracellular targets (*8*).

To gain insight into the role of tryptophan in IL-8α−target interactions, we performed intrinsic tryptophan fluorescence experiments in the presence of detergents and lipids. This approach was additionally helpful in providing one measure of the peptide position in both micelles and lipid bilayers, thus directly linking the solution and solid-state NMR work. The peptide penetrated to a very similar extent in all the anionic membrane mimetics, i.e., the SDS micelles and POPC/POPG SUVs, with the tryptophan well buried and inaccessible to the solvent. In contrast, the tryptophan residue penetrated less deeply into the zwitterionic POPC SUVs, remaining in a polar environment. These differences in penetration with model membrane composition are in keeping with the apparent preferential specificity of IL-8α for bacterial over mammalian membranes.

In addition to the tryptophan residue, IL-8α has one additional aromatic side chain, a phenylalanine at position 12. Like tryptophan, phenylalanine residues are known to be key residues in the antimicrobial activity of some peptides. For example, the phenylalanine location is critical for antibacterial activity in aurein 1.2 analogues (*76*). In tachyplesin I derivatives, the replacement of cysteines with phenylalanines leads to an increase in antimicrobial activity against fungi and *E. coli* (*77*). In the Pis-1 PG Piscidin 1 analogue, the insertion of phenylalanines into the membrane surface contributes to the anchoring of the peptide to the cell membrane (*78*). Likewise, in the IL-8α−SDS micelle complex, the phenylalanine 12 side chain orients itself in the same direction as the tryptophan side chain and is thus in a key position for strong interactions with the lipid acyl chains of bacterial cell membranes. Given the position of these two aromatic side chains within the peptide−micelle complex, (i.e., facing the interior of the micelle and at the end of the helix that is tilted more deeply into the micelle), it seems likely that these two residues may compensate in part for the reduced hydrophobicity and charge of IL-8α as compared to the average values for AMPs.

The current solution NMR studies provide detailed information about the peptide structure and its interactions with SDS micelles. Moreover, the tryptophan fluorescence experiments showed that the tryptophan residue adopts a similar position in both SDS micelles and POPC/POPG SUVs. Following from these observations, it was of interest to characterize in more detail the interaction of IL-8α peptide with lipid bilayers, which are more biologically relevant than micelles. Two model membranes were used. The first one consisted of POPC alone and was studied because this zwitterionic lipid is abundant in mammalian cell membranes. The second model membrane consisted of POPC and POPG at a 3/1 molar ratio, as POPG is an anionic lipid commonly found in bacterial plasma membranes, and the POPC/POPG mix has a membrane charge density similar to that of bacterial cytoplasmic membranes (*79*). The orientation of an antimicrobial peptide within the bilayer offers further insights into potential mechanisms of peptide membrane interaction and disruption that may contribute to AMP efficacy. Thus, the ^{15}N NMR spectrum of IL-8α was determined using mechanically oriented POPC/POPG bilayers. Most of the intensity in the ^{15}N spectrum was between 50 and 90 ppm (Figure 8), consistent with a largely in-plane orientation of the peptide within the bilayer, with a tilt angle in the realm of 0−15° (*80*). This orientation is consistent with the position of the peptide in SDS micelles, which was also found to be largely in-plane, but with a slight tilt of the N-terminus toward the micelle center. Such a parallel orientation of IL-8α tends to rule out the toroid pore and barrel stave mechanisms of membrane disruption (*81*, *82*), since these are thought to require a transmembrane orientation. On the contrary, if membrane disruption is a significant mechanistic determinant of IL-8α antimicrobial activity, these findings point more toward a carpet mechanism (*83*) or perhaps one of the mechanisms, such as the sinking raft, that have been proposed to involve only transient formation of distortions (*84*). However, it is possible that IL-8α and similar peptides have one or more antimicrobial effects through mechanisms that do not require significant initial or direct membrane perturbation (M. R. Yeaman et al., unpublished data).

As a complement to the studies described above, which focused on peptide structure and orientation, ^{2}H and ^{31}P solid-state NMR studies were used to assess the impact of IL-8α on the lipids in the oriented bilayers. The order parameter profiles derived from the ^{2}H spectra indicated a more peripheral interaction of the peptide with zwitterionic POPC bilayers and a deeper penetration into the anion-containing POPC/POPG bilayers. The addition of 3 mol % IL-8α to POPC-only bilayers led to a decrease in order parameters over the entire lipid chain length, consistent with a peripheral interaction of the peptide that increases the spacing between lipid headgroups and thus increases the degree of motional freedom of the chains (*85*, *86*). These results are consistent with the fluorescence experiments, which show an only peripheral interaction of IL-8α with POPC. Similar observations have been made for the antimicrobial peptide KIGAKI (*87*), in which fluorescence was not affected by addition of POPC, although there were decreases in lipid order (*88*). On the other hand, the ^{2}H order parameter profiles for POPC and POPG in the presence of 0 and 3% IL-8α were very similar, suggesting that the motions of the lipid acyl chains remain the same in the absence or presence of the peptide. This type of behavior has been interpreted as being indicative of a relatively deep location of the peptide in the lipid bilayer, where the peptide would constrain the motion of the lipid chains more than if it were located more peripherally within the bilayers (*87*, *89*, *90*). At 6 mol % IL-8α, the POPC/POPG ^{2}H order parameter profile is affected, perhaps indicating the acyl chain position might be saturated and the peptide might thus start to interact more peripherally with the lipid headgroups. The differences in IL-8α's interactions with the two model membranes are consistent with this peptide's putative preferential targeting of bacterial cells as compared to mammalian cells, as well as the tryptophan fluorescence results.

In neither POPC nor POPC/POPG bilayers with up to 6% peptide was there any evidence for nonlamellar-phase structures, such as cubic or hexagonal phases (Figure 5), or fragmentation of the bilayers to rapidly tumbling species such as micelles (Figure 6). The ^{2}H spectra (Figure 6) also provided no evidence of the formation of toroidal pores, which would give rise to a superposed spectrum at half the splitting observed, or significant membrane thinning, which could result in distortions to the observed spectra (*91*). These observations suggest a carpetlike mechanism of membrane disruption, rather than a pore or detergent type disruption. In fact, overall bilayer alignment was not significantly perturbed by the presence of IL-8α, as judged by the ^{2}H or ^{31}P NMR spectra (Figures 5 and 6). POPC bilayer alignment was not perturbed at all, even at 6 mol % peptide, and POPC/POPG bilayers were only very slightly perturbed at this peptide concentration. Additionally, the position of the ^{31}P peak did not shift significantly in the presence of peptide, indicating that IL-8α had no major effects on lipid headgroup tilt angle. Six mole percent is quite a high peptide/lipid ratio and comparable to the higher concentrations employed in many studies of AMPs that use oriented solid-state NMR, but since the antimicrobial assays with IL-8α (*28*) were performed in the solid phase, it is not possible to directly compare the peptide/lipid ratios between the functional and NMR studies; thus, we are not certain that 6 mol % is a "functional" concentration.

There are at least three potential reasons why an antimicrobial peptide might not perturb model lipid bilayers, as probed by solid-state NMR studies of oriented bilayers. First, its mechanism may involve little bilayer disruption, either because it only perturbs the membrane enough to cross it and gain access to an intracellular target or because its membrane-disrupting mechanism does not involve large-scale disruptions (*92*−*95*). Second, it is likely that at least some antimicrobial peptides act via mechanisms that involve only superficial interactions that trigger intracellular responses leading to target cell inhibition or death (*8*, *96*). Third, the membrane disrupting activities of an AMP may be highly dependent on membrane composition and thus not apparent in all model lipid systems. For example, Cheng et al. (*97*) found very modest effects with three aurein peptides on 3/1 POPC/POPG bilayers, versus much larger effects on bilayer disruption with DMPC/DMPG bilayers, which are thinner. Similarly, a Pardaxin peptide did not greatly disrupt POPC/POPG bilayers but significantly perturbed a number of other model lipid bilayers (*98*). Finally, a peptide based on granulysin, termed G15, was shown to have little effect on 3/1 POPC/POPG bilayers but a much stronger effect on bilayers made from *E. coli* lipid extract (*99*). This latter study is particularly interesting in comparison to our findings, as the G15 peptide has a charge and hydrophobicity very similar to those of IL-8α and, like IL-8α, contains a Trp and Phe residue positioned two helix turns apart from each other. Like IL-8α, G15 did not promote the formation of nonlamellar-phase structures or rapidly tumbling lipid structures, such as micelles. Hence, it is possible that IL-8α and G15 share a similar molecular mechanism of action that derives from their characteristic modest charge and hydrophobicity, as well as their shared Trp/Phe motif.

On balance, it is important to recognize the limitations of the observations reported herein. Studies employing model membranes like those presented in this work provide a necessary first stage for understanding mechanisms of antimicrobial peptides such as IL-8α. However, further work performed in the context of even more physiologically relevant systems, such as actual microbial and host cell membranes, is needed to more thoroughly elucidate the biological mechanism(s) of antimicrobial action of IL-8α or any AMP.

TRANSPARENCY STATEMENT

M.R.Y. is a shareholder of NovaDigm Therapeutics, Inc. He has received past research funding from Pfizer Inc., Amgen Inc., Cubist Pharmaceuticals, and Novozymes Pharmaceuticals. None of these entities provided support for this study.

ACKNOWLEDGMENT

We thank Stéphan Dubrau for his help in preparing Figure 1, Michael Hayley for suggesting the tryptophan fluorescence experiments, and Celine Schneider for NMR help, especially with the MAS experiments.

SUPPORTING INFORMATION AVAILABLE

Curve fitting for DOSY experiments (Figure 1) and ^{31}P MAS spectra of POPC in the absence and presence of 3 mol % IL-8α (Figure 2). This material is available free of charge via the Internet at http://pubs.acs.org.

REFERENCES

1. Shai, Y. (2002) Mode of action of membrane active antimicrobial peptides. *Biopolymers 66*, 236–248.
2. Mookherjee, N., and Hancock, R. E. (2007) Cationic host defence peptides: Innate immune regulatory peptides as a novel approach for treating infections. *Cell. Mol. Life Sci. 64*, 922–933.

3. Cole, A. M., Ganz, T., Liese, A. M., Burdick, M. D., Liu, L., and Strieter, R. M. (2001) Cutting edge: IFN-inducible ELR-CXC chemokines display defensin-like antimicrobial activity. *J. Immunol. 167*, 623–627.
4. Durr, M., and Peschel, A. (2002) Chemokines meet defensins: The merging concepts of chemoattractants and antimicrobial peptides in host defense. *Infect. Immun. 70*, 6515–6517.
5. Clore, G. M., Appella, E., Yamada, M., Matsushima, K., and Gronenborn, A. M. (1990) Three-dimensional structure of interleukin 8 in solution. *Biochemistry 29*, 1689–1696.
6. Rajarathnam, K., Clark-Lewis, I., and Sykes, B. D. (1995) ^{1}H NMR solution structure of an active monomeric interleukin-8. *Biochemistry 34*, 12983–12990.
7. Baldwin, E. T., Weber, I. T., St Charles, R., Xuan, J. C., Appella, E., Yamada, M., Matsushima, K., Edwards, B. F., Clore, G. M., and Gronenborn, A. M..; et al. (1991) Crystal structure of interleukin 8: Symbiosis of NMR and crystallography. *Proc. Natl. Acad. Sci. U.S.A. 88*, 502–506.
8. Yeaman, M. R., and Yount, N. Y. (2003) Mechanisms of antimicrobial peptide action and resistance. *Pharmacol. Rev. 55*, 27–55.
9. De Smet, K., and Contreras, R. (2005) Human antimicrobial peptides: Defensins, cathelicidins and histatins. *Biotechnol. Lett. 27*, 1337–1347.
10. Pazgier, M., Li, X., Lu, W., and Lubkowski, J. (2007) Human defensins: Synthesis and structural properties. *Curr. Pharm. Des. 13*, 3096–3118.
11. Tang, Y. Q., Yeaman, M. R., and Selsted, M. E. (1995) Purification, characterization, and antimicrobial properties of peptides released from thrombin-induced human platelets. *Blood 86*, 910a.
12. Yeaman, M. R., Tang, Y. Q., Shen, A. J., Bayer, A. S., and Selsted, M. E. (1997) Purification and in vitro activities of rabbit platelet microbicidal proteins. *Infect. Immun. 65*, 1023–1031.
13. Crawford, M. A., Zhu, Y., Green, C. S., Burdick, M. D., Sanz, P., Alem, F., O'Brien, A. D., Mehrad, B., Strieter, R. M., and Hughes, M. A. (2009) Antimicrobial effects of interferon-inducible CXC chemokines against *Bacillus anthracis* spores and bacilli. *Infect. Immun. 77*, 1664–1678.
14. Yount, N. Y., Waring, A. J., Gank, K. D., Welch, W. H., Kupferwasser, D., and Yeaman, M. R. (2007) Structural correlates of antimicrobial efficacy in IL-8 and related human kinocidins. *Biochim. Biophys. Acta 1768*, 598–608.
15. Yang, D., Chen, Q., Hoover, D. M., Staley, P., Tucker, K. D., Lubkowski, J., and Oppenheim, J. J. (2003) Many chemokines including CCL20/MIP-3α display antimicrobial activity. *J. Leukocyte Biol. 74*, 448–455.
16. Hieshima, K., Ohtani, H., Shibano, M., Izawa, D., Nakayama, T., Kawasaki, Y., Shiba, F., Shiota, M., Katou, F., Saito, T., and Yoshie, O. (2003) CCL28 has dual roles in mucosal immunity as a chemokine with broad-spectrum antimicrobial activity. *J. Immunol. 170*, 1452–1461.
17. Linge, H. M., Collin, M., Nordenfelt, P., Morgelin, M., Malmsten, M., and Egesten, A. (2008) The human CXC chemokine granulocyte chemotactic protein 2 (GCP-2)/CXCL6 possesses membrane-disrupting properties and is antibacterial. *Antimicrob. Agents Chemother. 52*, 2599–2607.
18. Maerki, C., Meuter, S., Liebi, M., Muhlemann, K., Frederick, M. J., Yawalkar, N., Moser, B., and Wolf, M. (2009) Potent and broad-spectrum antimicrobial activity of CXCL14 suggests an immediate role in skin infections. *J. Immunol. 182*, 507–514.
19. Krijgsveld, J., Zaat, S. A., Meeldijk, J., van Veelen, P. A., Fang, G., Poolman, B., Brandt, E., Ehlert, J. E., Kuijpers, A. J., Engbers, G. H., Feijen, J., and Dankert, J. (2000) Thrombocidins, microbicidal proteins from human blood platelets, are C-terminal deletion products of CXC chemokines. *J. Biol. Chem. 275*, 20374–20381.
20. Martinez-Becerra, F., Silva, D. A., Dominguez-Ramirez, L., Mendoza-Hernandez, G., Lopez-Vidal, Y., Soldevila, G., and Garcia-Zepeda, E. A. (2007) Analysis of the antimicrobial activities of a chemokine-derived peptide (CDAP-4) on *Pseudomonas aeruginosa*. *Biochem. Biophys. Res. Commun. 355*, 352–358.
21. Tang, Y. Q., Yeaman, M. R., and Selsted, M. E. (2002) Antimicrobial peptides from human platelets. *Infect. Immun. 70*, 6524–6533.
22. Yeaman, M. R., Gank, K. D., Bayer, A. S., and Brass, E. P. (2002) Synthetic peptides that exert antimicrobial activities in whole blood and blood-derived matrices. *Antimicrob. Agents Chemother. 46*, 3883–3891.
23. Yount, N. Y., Gank, K. D., Xiong, Y. Q., Bayer, A. S., Pender, T., Welch, W. H., and Yeaman, M. R. (2004) Platelet microbicidal protein 1: Structural themes of a multifunctional antimicrobial peptide. *Antimicrob. Agents Chemother. 48*, 4395–4404.
24. Yount, N. Y., Andrés, M. T., Fierro, J. F., and Yeaman, M. R. (2007) The γ-core motif correlates with antimicrobial activity in cysteine-containing kaliocin-1 originating from transferrins. *Biochim. Biophys. Acta 1768*, 2862–2872.
25. Yeaman, M. R., Yount, N. Y., Waring, A. J., Gank, K. D., Kupferwasser, D., Wiese, R., Bayer, A. S., and Welch, W. H. (2007) Modular determinants of antimicrobial activity in platelet factor-4 family kinocidins. *Biochim. Biophys. Acta 1768*, 609–619.
26. Xiong, Y. Q., Yeaman, M. R., and Bayer, A. S. (1999) In vitro antibacterial activities of platelet microbicidal protein and neutrophil defensin against *Staphylococcus aureus* are influenced by antibiotics differing in mechanism of action. *Antimicrob. Agents Chemother. 43*, 1111–1117.
27. Yeaman, M. R., Bayer, A. S., Koo, S. P., Foss, W., and Sullam, P. M. (1998) Platelet microbicidal proteins and neutrophil defensin disrupt the *Staphylococcus aureus* cytoplasmic membrane by distinct mechanisms of action. *J. Clin. Invest. 101*, 178–187.
28. Björstad, A., Fu, H., Karlsson, A., Dahlgren, C., and Bylund, J. (2005) Interleukin-8-derived peptide has antibacterial activity. *Antimicrob. Agents Chemother. 49*, 3889–3895.
29. Gallo, R. L., Murakami, M., Ohtake, T., and Zaiou, M. (2002) Biology and clinical relevance of naturally occurring antimicrobial peptides. *J. Allergy Clin. Immunol. 110*, 823–831.
30. Yeaman, M. R., and Yount, N. Y. (2005) Code among chaos: Immunorelativity and the AEGIS model of antimicrobial peptides. *ASM News 71*, 21–27.
31. Lee, D. G., Kim, H. K., Kim, S. A., Park, Y., Park, S. C., Jang, S. H., and Hahm, K. S. (2003) Fungicidal effect of indolicidin and its interaction with phospholipid membranes. *Biochem. Biophys. Res. Commun. 305*, 305–310.
32. Lee, I. H., Cho, Y., and Lehrer, R. I. (1997) Effects of pH and salinity on the antimicrobial properties of clavanins. *Infect. Immun. 65*, 2898–2903.
33. Bourbigot, S., Dodd, E., Horwood, C., Cumby, N., Fardy, L., Welch, W. H., Ramjan, Z., Sharma, S., Waring, A. J., Yeaman, M. R., and Booth, V. (2009) Antimicrobial peptide RP-1 structure and interactions with anionic versus zwitterionic micelles. *Biopolymers 91*, 1–13.
34. Delaglio, F., Grzesiek, S., Vuister, G. W., Zhu, G., Pfeifer, J., and Bax, A. (1995) NMRPipe: A multidimensional spectral processing system based on UNIX pipes. *J. Biomol. NMR 6*, 277–293.
35. Goddard, T. D., and Kneller, D. G. (2005) SPARKY 3 , University of California, San Francisco.
36. Wuthrich, K. (1986) NMR of Proteins and Nucleic Acids , John Wiley & Sons, New York.
37. Clore, G. M., Nilges, M., Sukumaran, D. K., Brunger, A. T., Karplus, M., and Gronenborn, A. M. (1986) The three-dimensional structure of α1-purothionin in solution: Combined use of nuclear magnetic resonance, distance geometry and restrained molecular dynamics. *EMBO J. 5*, 2729–2735.
38. Brunger, A. T., Adams, P. D., Clore, G. M., DeLano, W. L., Gros, P., Grosse-Kunstleve, R. W., Jiang, J. S., Kuszewski, J., Nilges, M., Pannu, N. S., Read, R. J., Rice, L. M., Simonson, T., and Warren, G. L. (1998) Crystallography & NMR system: A new software suite for macromolecular structure determination. *Acta Crystallogr. D54*, 905–921.
39. Laskowski, R. A., Rullmannn, J. A., MacArthur, M. W., Kaptein, R., and Thornton, J. M. (1996) AQUA and PROCHECK-NMR: Programs for checking the quality of protein structures solved by NMR. *J. Biomol. NMR 8*, 477–486.
40. Morris, A. L., MacArthur, M. W., Hutchinson, E. G., and Thornton, J. M. (1992) Stereochemical quality of protein structure coordinates. *Proteins 12*, 345–364.
41. Koradi, R., Billeter, M., and Wuthrich, K. (1996) MOLMOL: A program for display and analysis of macromolecular structures. *J. Mol. Graphics 14* (51−5), 29–32.
42. Guex, N., and Peitsch, M. C. (1997) SWISS-MODEL and the Swiss-PdbViewer: An environment for comparative protein modeling. *Electrophoresis 18*, 2714–2723.
43. Morris, K. F., and Johnson, C. S.Jr. (1992) Diffusion-ordered two-dimensional nuclear magnetic resonance spectroscopy. *J. Am. Chem. Soc. 114*, 3139–3141.
44. Tanner, J. E. (1970) Use of the Stimulated Echo in NMR Diffusion Studies. *J. Chem. Phys. 52*, 2523–2526.
45. Sklenar, V., Piotto, M., Leppik, R., and Saudek, V. (1993) Gradient-Tailored Water Suppression for ^{1}H-^{15}N HSQC Experiments Optimized to Retain Full Sensitivity. *J. Magn. Reson., Ser. A 102*, 241–245.
46. Bennett, A. E., Rienstra, C. M., Auger, M., Lakshmi, K. V., and Griffin, R. G. (1995) Heteronuclear decoupling in rotating solids. *J. Chem. Phys. 103*, 6951–6958.

47. Sternin, E., Fine, B., Bloom, M., Tilcock, C. P., Wong, K. F., and Cullis, P. R. (1988) Acyl chain orientational order in the hexagonal HII phase of phospholipid-water dispersions. *Biophys. J. 54*, 689–694.
48. Burnett, L. J., and Muller, B. H. (1971) Deuteron Quadrupole Coupling Constants in Three Solid Deuterated Paraffin Hydrocarbons: C2D6, C4D10, C6D14. *J. Chem. Phys. 55*, 5829–5831.
49. Eftink, M. R., and Ghiron, C. A. (1976) Exposure of tryptophanyl residues in proteins. Quantitative determination by fluorescence quenching studies. *Biochemistry 15*, 672–680.
50. Kelly, S. M., Jess, T. J., and Price, N. C. (2005) How to study proteins by circular dichroism. *Biochim. Biophys. Acta 1751*, 119–139.
51. Wishart, D. S., Bigam, C. G., Holm, A., Hodges, R. S., and Sykes, B. D. (1995) ^{1}H, ^{13}C and ^{15}N random coil NMR chemical shifts of the common amino acids. I. Investigations of nearest-neighbor effects. *J. Biomol. NMR 5*, 67–81.
52. Hayter, J. B., and Penfold, J. (1981) Self-consistent structural and dynamic study of concentrated micelle solutions. *J. Chem. Soc., Faraday Trans. 1* (77), 1851–1863.
53. Itri, R., and Amaral, L. Q. (1991) Distance distribution function of sodium dodecyl sulfate micelles by X-ray scattering. *J. Phys. Chem. 95*, 423–427.
54. Whitehead, T. L., Jones, L. M., and Hicks, R. P. (2001) Effects of the incorporation of CHAPS into SDS micelles on neuropeptide-micelle binding: Separation of the role of electrostatic interactions from hydrophobic interactions. *Biopolymers 58*, 593–605.
55. Stilbs, P. (1982) Fourier transform NMR pulsed-gradient spin-echo (FT-PGSE) self-diffusion measurements of solubilization equilibria in SDS solutions. *J. Colloid Interface Sci. 87*, 385–394.
56. Papavoine, C. H., Konings, R. N., Hilbers, C. W., and van de Ven, F. J. (1994) Location of M13 coat protein in sodium dodecyl sulfate micelles as determined by NMR. *Biochemistry 33*, 12990–12997.
57. Zamoon, J., Mascioni, A., Thomas, D. D., and Veglia, G. (2003) NMR solution structure and topological orientation of monomeric phospholamban in dodecylphosphocholine micelles. *Biophys. J. 85*, 2589–2598.
58. Surewicz, W. K., and Epand, R. M. (1984) Role of peptide structure in lipid-peptide interactions: A fluorescence study of the binding of pentagastrin-related pentapeptides to phospholipid vesicles. *Biochemistry 23*, 6072–6077.
59. Lakowicz, J. R., and Masters, B. R. (2008) Principles of fluorescence spectroscopy. *J. Biomed. Opt. 13*, 029901.
60. Bechinger, B., and Sizun, C. (2003) Alignment and structural analysis of membrane polypeptides by ^{15}N and ^{31}P solid-state NMR spectroscopy. *Concepts Magn. Reson. 18*, 130–145.
61. Wang, G., Li, X., and Wang, Z. (2009) APD2: The updated antimicrobial peptide database and its application in peptide design. *Nucleic Acids Res. 37*, D933–D937.
62. Bello, J., Bello, H. R., and Granados, E. (1982) Conformation and aggregation of melittin: Dependence on pH and concentration. *Biochemistry 21*, 461–465.
63. Dathe, M., and Wieprecht, T. (1999) Structural features of helical antimicrobial peptides: Their potential to modulate activity on model membranes and biological cells. *Biochim. Biophys. Acta 1462*, 71–87.
64. de Planque, M. R., Kruijtzer, J. A., Liskamp, R. M., Marsh, D., Greathouse, D. V., Koeppe, R. E., de Kruijff, B., and Killian, J. A. (1999) Different membrane anchoring positions of tryptophan and lysine in synthetic transmembrane α-helical peptides. *J. Biol. Chem. 274*, 20839–20846.
65. Johnston, J. M., Cook, G. A., Tomich, J. M., and Sansom, M. S. (2006) Conformation and environment of channel-forming peptides: A simulation study. *Biophys. J. 90*, 1855–1864.
66. de Planque, M. R., Boots, J. W., Rijkers, D. T., Liskamp, R. M., Greathouse, D. V., and Killian, J. A. (2002) The effects of hydrophobic mismatch between phosphatidylcholine bilayers and transmembrane α-helical peptides depend on the nature of interfacially exposed aromatic and charged residues. *Biochemistry 41*, 8396–8404.
67. Kyte, J., and Doolittle, R. F. (1982) A simple method for displaying the hydropathic character of a protein. *J. Mol. Biol. 157*, 105–132.
68. Wimley, W. C., and White, S. H. (1996) Experimentally determined hydrophobicity scale for proteins at membrane interfaces. *Nat. Struct. Biol. 3*, 842–848.
69. Schibli, D. J., Epand, R. F., Vogel, H. J., and Epand, R. M. (2002) Tryptophan-rich antimicrobial peptides: Comparative properties and membrane interactions. *Biochem. Cell Biol. 80*, 667–677.
70. Schibli, D. J., Montelaro, R. C., and Vogel, H. J. (2001) The membrane-proximal tryptophan-rich region of the HIV glycoprotein, gp41, forms a well-defined helix in dodecylphosphocholine micelles. *Biochemistry 40*, 9570–9578.
71. Schiffer, M., Chang, C. H., and Stevens, F. J. (1992) The functions of tryptophan residues in membrane proteins. *Protein Eng. 5*, 213–214.
72. Stopar, D., Spruijt, R. B., and Hemminga, M. A. (2006) Anchoring mechanisms of membrane-associated M13 major coat protein. *Chem. Phys. Lipids 141*, 83–93.
73. Rezansoff, A. J., Hunter, H. N., Jing, W., Park, I. Y., Kim, S. C., and Vogel, H. J. (2005) Interactions of the antimicrobial peptide Ac-FRWWHR-NH_2 with model membrane systems and bacterial cells. *J. Pept. Res. 65*, 491–501.
74. Hunter, H. N., Jing, W., Schibli, D. J., Trinh, T., Park, I. Y., Kim, S. C., and Vogel, H. J. (2005) The interactions of antimicrobial peptides derived from lysozyme with model membrane systems. *Biochim. Biophys. Acta 1668*, 175–189.
75. Strom, M. B., Rekdal, O., and Svendsen, J. S. (2000) Antibacterial activity of 15-residue lactoferricin derivatives. *J. Pept. Res. 56*, 265–274.
76. Li, X., Li, Y., Peterkofsky, A., and Wang, G. (2006) NMR studies of aurein 1.2 analogs. *Biochim. Biophys. Acta 1758*, 1203–1214.
77. Rao, A. G. (1999) Conformation and antimicrobial activity of linear derivatives of tachyplesin lacking disulfide bonds. *Arch. Biochem. Biophys. 361*, 127–134.
78. Lee, S. A., Kim, Y. K., Lim, S. S., Zhu, W. L., Ko, H., Shin, S. Y., Hahm, K. S., and Kim, Y. (2007) Solution structure and cell selectivity of piscidin 1 and its analogues. *Biochemistry 46*, 3653–3663.
79. Ratledge, C., and Wilkinson, S. G. *Microbial Lipids*, Academic Press: London, 1988.
80. Bechinger, B., Aisenbrey, C., and Bertani, P. (2004) The alignment, structure and dynamics of membrane-associated polypeptides by solid-state NMR spectroscopy. *Biochim. Biophys. Acta 1666*, 190–204.
81. Ludtke, S. J., He, K., Heller, W. T., Harroun, T. A., Yang, L., and Huang, H. W. (1996) Membrane pores induced by magainin. *Biochemistry 35*, 13723–13728.
82. Matsuzaki, K., Murase, O., Fujii, N., and Miyajima, K. (1996) An antimicrobial peptide, magainin 2, induced rapid flip-flop of phospholipids coupled with pore formation and peptide translocation. *Biochemistry 35*, 11361–11368.
83. Pouny, Y., Rapaport, D., Mor, A., Nicolas, P., and Shai, Y. (1992) Interaction of antimicrobial dermaseptin and its fluorescently labeled analogues with phospholipid membranes. *Biochemistry 31*, 12416–12423.
84. Chan, D. I., Prenner, E. J., and Vogel, H. J. (2006) Tryptophan- and arginine-rich antimicrobial peptides: Structures and mechanisms of action. *Biochim. Biophys. Acta 1758*, 1184–1202.
85. Mecke, A., Lee, D. K., Ramamoorthy, A., Orr, B. G., and Banaszak Holl, M. M. (2005) Membrane thinning due to antimicrobial peptide binding: An atomic force microscopy study of MSI-78 in lipid bilayers. *Biophys. J. 89*, 4043–4050.
86. Henzler-Wildman, K. A., Martinez, G. V., Brown, M. F., and Ramamoorthy, A. (2004) Perturbation of the hydrophobic core of lipid bilayers by the human antimicrobial peptide LL-37. *Biochemistry 43*, 8459–8469.
87. Lu, J. X., Damodaran, K., Blazyk, J., and Lorigan, G. A. (2005) Solid-state nuclear magnetic resonance relaxation studies of the interaction mechanism of antimicrobial peptides with phospholipid bilayer membranes. *Biochemistry 44*, 10208–10217.
88. Jin, Y., Mozsolits, H., Hammer, J., Zmuda, E., Zhu, F., Zhang, Y., Aguilar, M. I., and Blazyk, J. (2003) Influence of tryptophan on lipid binding of linear amphipathic cationic antimicrobial peptides. *Biochemistry 42*, 9395–9405.
89. Antharam, V. C., Farver, R. S., Kuznetsova, A., Sippel, K. H., Mills, F. D., Elliott, D. W., Sternin, E., and Long, J. R. (2008) Interactions of the C-terminus of lung surfactant protein B with lipid bilayers are modulated by acyl chain saturation. *Biochim. Biophys. Acta 1778*, 2544–2554.
90. Koenig, B. W., Ferretti, J. A., and Gawrisch, K. (1999) Site-specific deuterium order parameters and membrane-bound behavior of a peptide fragment from the intracellular domain of HIV-1 gp41. *Biochemistry 38*, 6327–6334.
91. Wi, S., and Kim, C. (2008) Pore structure, thinning effect, and lateral diffusive dynamics of oriented lipid membranes interacting with antimicrobial peptide protegrin-1: ^{31}P and ^{2}H solid-state NMR study. *J. Phys. Chem. B 112*, 11402–11414.

92. Brogden, K. A. (2005) Antimicrobial peptides: Pore formers or metabolic inhibitors in bacteria? *Nat. Rev. Microbiol. 3*, 238–250.
93. Jenssen, H., Hamill, P., and Hancock, R. E. (2006) Peptide antimicrobial agents. *Clin. Microbiol. Rev. 19*, 491–511.
94. Bechinger, B. (1999) The structure, dynamics and orientation of antimicrobial peptides in membranes by multidimensional solid-state NMR spectroscopy. *Biochim. Biophys. Acta 1462*, 157–183.
95. Oren, Z., Hong, J., and Shai, Y. (1997) A repertoire of novel antibacterial diastereomeric peptides with selective cytolytic activity. *J. Biol. Chem. 272*, 14643–14649.
96. Yeaman, M. R., and Yount, N. Y. (2007) Unifying themes in host defence effector polypeptides. *Nat. Rev. Microbiol. 5*, 727–740.
97. Cheng, J. T., Hale, J. D., Elliot, M., Hancock, R. E., and Straus, S. K. (2009) Effect of membrane composition on antimicrobial peptides aurein 2.2 and 2.3 from Australian southern bell frogs. *Biophys. J. 96*, 552–565.
98. Hallock, K. J., Lee, D. K., Omnaas, J., Mosberg, H. I., and Ramamoorthy, A. (2002) Membrane composition determines pardaxin's mechanism of lipid bilayer disruption. *Biophys. J. 83*, 1004–1013.
99. Ramamoorthy, A., Thennarasu, S., Tan, A., Lee, D. K., Clayberger, C., and Krensky, A. M. (2006) Cell selectivity correlates with membrane-specific interactions: A case study on the antimicrobial peptide G15 derived from granulysin. *Biochim. Biophys. Acta 1758*, 154–163.